J Neurophysiol 119: 1209–1221, 2018.
First published December 13, 2017; doi:10.1152/jn.00082.2017.

RESEARCH ARTICLE | *Sensory Processing*

Bayesian quantification of sensory reweighting in a familial bilateral vestibular disorder (DFNA9)

Bart B. G. T. Alberts,[1] Luc P. J. Selen,[1] Wim I. M. Verhagen,[2] Ronald J. E. Pennings,[1,3] and W. Pieter Medendorp[1]

[1]*Donders Institute for Brain, Cognition and Behaviour, Radboud University Nijmegen, Nijmegen, The Netherlands;* [2]*Neurology, Canisius Wilhelmina Hospital, Nijmegen, The Netherlands; and* [3]*Department of Otorhinolaryngology, Radboud University Medical Centre, Nijmegen, The Netherlands*

Submitted 8 February 2017; accepted in final form 6 December 2017

Alberts BB, Selen LP, Verhagen WI, Pennings RJ, Medendorp WP. Bayesian quantification of sensory reweighting in a familial bilateral vestibular disorder (DFNA9). *J Neurophysiol* 119: 1209–1221, 2018. First published December 13, 2017; doi:10.1152/jn.00082.2017.—DFNA9 is a rare progressive autosomal dominantly inherited vestibulo-cochlear disorder, resulting in a homogeneous group of patients with hearing impairment and bilateral vestibular function loss. These patients suffer from a deteriorated sense of spatial orientation, leading to balance problems in darkness, especially on irregular surfaces. Both behavioral and functional imaging studies suggest that the remaining sensory cues could compensate for the loss of vestibular information. A thorough model-based quantification of this reweighting in individual patients is, however, missing. Here we psychometrically examined the individual patient's sensory reweighting of these cues after complete vestibular loss. We asked a group of DFNA9 patients and healthy control subjects to judge the orientation (clockwise or counterclockwise relative to gravity) of a rod presented within an oriented square frame (rod-in-frame task) in three different head-on-body tilt conditions. Our results show a cyclical frame-induced bias in perceived gravity direction across a 90° range of frame orientations. The magnitude of this bias was significantly increased in the patients compared with the healthy control subjects. Response variability, which increased with head-on-body tilt, was also larger for the patients. Reverse engineering of the underlying signal properties, using Bayesian inference principles, suggests a reweighting of sensory signals, with an increase in visual weight of 20–40% in the patients. Our approach of combining psychophysics and Bayesian reverse engineering is the first to quantify the weights associated with the different sensory modalities at an individual patient level, which could make it possible to develop personal rehabilitation programs based on the patient's sensory weight distribution.

NEW & NOTEWORTHY It has been suggested that patients with vestibular deficits can compensate for this loss by increasing reliance on other sensory cues, although an actual quantification of this reweighting is lacking. We combine experimental psychophysics with a reverse engineering approach based on Bayesian inference principles to quantify sensory reweighting in individual vestibular patients. We discuss the suitability of this approach for developing personal rehabilitation programs based on the patient's sensory weight distribution.

Address for reprint requests and other correspondence: W. P. Medendorp, Radboud Univ., Donders Inst. for Brain, Cognition and Behaviour, Nijmegen, Montessorilaan 3 B01.40, 6525HR Nijmegen, The Netherlands (e-mail: p.medendorp@donders.ru.nl).

bilateral vestibular areflexia; internal models; multisensory integration; rod-frame illusion; spatial orientation; verticality perception

INTRODUCTION

Accurate perception of gravity is important for spatial orientation, postural balance, and the regulation of gait. Multiple sensory signals contribute to the central processing of this percept, including signals from visual, vestibular, and somatosensory systems (Angelaki and Cullen 2008; Carriot et al. 2011; Lackner and DiZio 2005; Mittelstaedt 1992, 1995, 1996). These sensory signals may be supplemented by cognitive signals that reflect previously experienced head orientations, as we and others have suggested before (Clemens et al. 2011; De Vrijer et al. 2008; MacNeilage et al. 2007; Van Barneveld et al. 2011).

How multiple sensory and cognitive signals are integrated to provide a percept of gravity direction is difficult to establish. One reason is that the contribution of each of the signals cannot be isolated. For example, roll tilting the head is detected not only by neck proprioceptors but also by vestibular sensors located in the inner ear. Another reason is that cues may be in conflict with each other; for example, visual cues could conflict with graviceptive information provided by the otoliths and pressure receptors (Eggert 1992, 1998; Li and Matin 2005a, 2005b; Matin and Li 1995; Vingerhoets et al. 2009). A third reason is that sensory signals are often ambiguous, e.g., the otoliths cannot distinguish gravity from other linear accelerations (Angelaki and Yakusheva 2009; Fernández and Goldberg 1976). A final reason is that sensory and neural signals are inherently noisy, the level of which may depend on the strength of the signal (Clark et al. 2015; Faisal et al. 2008; Sober and Körding 2012). All of these factors have some interplay in the integration process, which in turn influences activity at central levels.

This integration process is often said to be flawed, because our perception of gravity is distorted, especially when we are tilted or in motion (Alberts et al. 2016; Aubert 1861; Clemens et al. 2011; Mittelstaedt 1983; Tarnutzer et al. 2010). However, recent modeling studies have suggested that these perceptual distortions are the result of an optimal multimodal integration process for gravity perception that involves Bayesian inference (Clemens et al. 2011;

Eggert 1998; MacNeilage et al. 2007). In such a framework, the brain is supposed to combine prior beliefs with noisy, ambiguous, and conflicting data when perceiving the gravitational environment. Using this framework, we were able to explain the systematic errors in gravity perception that subjects show when tilted (Alberts et al. 2016; Clemens et al. 2011; De Vrijer et al. 2008) but also the systematic errors in gravity perception when vision provides conflicting cues (Alberts et al. 2016; Vingerhoets et al. 2009). This probabilistic framework further explains changes in verticality perception due to sensory reweighting when sensory noise levels change because of aging, disease (Alberts et al. 2016; Anson and Jeka 2016; Clemens et al. 2011), or artificial manipulations (Mars et al. 2001; Santos-Pontelli et al. 2016; Volkening et al. 2014). Here we assess the role of sensory reweighting in response to complete, but gradually acquired, loss of bilateral vestibular function in a homogeneous group of DFNA9 patients.

DFNA9 is a progressive autosomal dominant vestibulocochlear disorder, resulting in hearing impairment and vestibular function loss (Cremers et al. 2005; Huygen et al. 1989, 1991; Verhagen et al. 2000). Histopathology in advanced disease shows severe atrophy of cochlear and vestibular nerve endings due to an acidophilic mucopolysaccharide deposit, identified in the cochlea and macula (Verhagen et al. 2000). These patients further show neuroepithelial and neural degeneration in the inner ear (Robertson et al. 2006). The DFNA9 mutation does not affect the proprioceptive or visual system and the functioning of the brain.

Measuring visual dependence is a method used to characterize vestibular patients. It has been shown that patients with vestibular areflexia are more affected by visual cues when reporting the gravitational vertical (Bronstein 1999; Bronstein et al. 1996; Grabherr et al. 2011; Guerraz et al. 2001; Lopez et al. 2007). These studies reported that optokinetic roll stimuli and static frames induce stronger biases in the percept of vertical in vestibular patients than in healthy control subjects, as though patients rely more on visual information. Likewise, functional imaging studies have illustrated enhanced cortical visual activation in such patients (Cutfield et al. 2014; Dieterich et al. 2007). Patients with vestibular areflexia also rely more on cervical proprioceptive, body somatosensory, and other nonvestibular signals. For example, cervical-ocular reflex gains are increased (Bronstein and Hood 1986; Gresty et al. 1977; Huygen et al. 1991; Kasai and Zee 1978) and vibration of the cervical muscles induces a stronger change in head-on-body orientation percept in patients compared with healthy control subjects (Popov et al. 1996). In 2015, we demonstrated a stronger reliance on somatosensory cues when DFNA9 patients had to report their body orientation in space in darkness, and thus without visual cues (Alberts et al. 2015).

Thus we suggested that DFNA9 patients have learned to compensate for the loss of direct vestibular cues by increasing reliance on visual and other nonvestibular cues (Alberts et al. 2015; Huygen et al. 1989, 1991; Huygen and Verhagen 2011). Although behavioral and imaging studies hint at a reweighting of these remaining sensory cues, a thorough model-based quantification of this reweighting is lacking. Estimation of the weights requires a good quantitative measure of variability. It is well known that adjustment methods, even though easy and intuitively appealing approaches, are subjective and can produce unreliable results (see Lewis 2015; Merfeld 2011 for further considerations).

Here we fill this gap in the literature by combining experimental psychophysics with a reverse engineering approach to quantify sensory reweighting in individual DFNA9 patients and healthy control subjects. We use a rod-and-frame task, in combination with head tilt, to determine the contributions of visual, vestibular, and nonvestibular signals to gravity perception (Bagust 2005; Beh et al. 1971; Beh and Wenderoth 1972; Mars et al. 2004; Matin and Li 1995; Witkin and Asch 1948). On the basis of optimal Bayesian inference principles we reverse engineered the noise characteristics of the sensory modalities and quantified the weights of the visual and nonvestibular cues for individual patients (and control subjects). This personalized quantification may contribute to development of rehabilitation programs that are tailored to and based on the patient's sensory weight distribution.

MATERIALS AND METHODS

Subjects. A homogeneous group of 16 naive bilateral vestibular areflexic patients (13 women, 3 men; age 65.1 ± 8.0 yr) and 16 healthy age-matched control subjects (13 women, 3 men; age 58.4 ± 10.5 yr) participated in the experiment. All patients showed complete loss of vestibular function due to a hereditary progressive vestibulocochlear dysfunction caused by a *COCH* gene mutation (DFNA9) (Verhagen et al. 2000). While the patients in this study are from different families, a common ancestor is likely (Fransen et al. 2001). Although vestibular function was completely lost, patients still had a small amount of remaining auditory function, enhanced by hearing aids ($n = 7$) or restored by cochlear implants ($n = 7$ on right side, $n = 2$ on left side). Typically, vestibular loss precedes total hearing loss in DFNA9, and from the age of 54 yr onward all patients show bilateral vestibular areflexia (Bischoff et al. 2005). Performance on vestibular tests is described below (see *Vestibular testing*). Integrity of the vestibular system in control subjects was not clinically tested, but subjects reported being free of any known vestibular or other neurological disorders. One patient suffered from diabetes mellitus with a mild polyneuropathy, but the other patients had no additional neurological abnormalities. All subjects had normal or corrected to normal vision. Both groups, patients and control subjects, gave written informed consent to the guidelines of the local ethics committee of the Social Sciences Faculty of Radboud University, which approved the study. Before the experiment, subjects were carefully instructed about the different tasks. Subjects never received feedback about their performance.

Vestibular testing. Table 1 reports the findings of several clinical tests performed to confirm complete vestibular loss. In some patients we did not perform all tests, but they could be classified as having bilateral vestibular areflexia on the basis of DNA testing and physical examination, taking their age also into account (Bischoff et al. 2005).

Besides genetic confirmation through mutation analysis of the *COCH* gene, we performed various otolith tests, canal tests, and indirect vestibular tests. Otolith function was tested by rotating patients at constant velocity during 4-cm eccentric off-axis rotation (i.e., the head's rotation axis was 4 cm lateral to the center of the interaural axis in the direction of the ear). Absence of ocular counterroll indicated a complete loss of the otolith signal. Furthermore, myogenic potentials due to bone vibration of the head were recorded by surface EMG electrodes underneath the eyes (oVEMP) and at the sternocleidomastoid muscles (cVEMP, both air conducted and bone conducted). Loss of both utricular (oVEMP) and saccular (cVEMP) function was confirmed by the absence of myogenic potentials. Absence of ocular counterrolling (OCR) when the head was statically tilted on the trunk to 25° confirmed these observations.

Absence of postrotary nystagmus responses during velocity step tests, with rotational velocities of 90°/s and 250°/s, indicated complete loss of the lateral semicircular canal. This was confirmed by absence

Table 1. *Clinical tests performed to show vestibular areflexia*

	Patient 1	*Patient 2*	*Patient 3*	*Patient 4*	*Patient 5*	*Patient 6*	*Patient 7*	*Patient 8*
Otolith tests								
Age	73	49	68	68	73	66	62	71
4 cm off-axis rotation	No OCR	—	No OCR	—	No OCR	—	—	—
oVEMP	No response	No response	No response	—	—	—	—	—
cVEMP	No response	No response	No response	—	—	—	—	—
OCR video	No OCR	No OCR	No OCR	No OCR	No OCR	—	—	—
Canal tests								
Video head impulse test	Catch-up saccades (no VOR)	Catch-up saccades (no VOR)	Catch-up saccades (no VOR)	Catch-up saccades (no VOR)	Catch-up saccades (no VOR)	Catch-up saccades (no VOR)	Catch-up saccades (no VOR)	Catch-up saccades (no VOR)
VOR (90°) step test	No postrotary nystagmus	No postrotary nystagmus	No postrotary nystagmus	No postrotary nystagmus	No postrotary nystagmus	No postrotary nystagmus	—	No postrotary nystagmus
VOR (250°) step test	No postrotary nystagmus	—	No postrotary nystagmus	No postrotary nystagmus	No postrotary nystagmus	—	—	—
Caloric test (30 and 44°C)	No reactive eye movements	No reactive eye movements	No reactive eye movements	No reactive eye movements	No reactive eye movements	—	—	—
Other tests								
DNA testing	p.Pro51Ser	p.Pro51Ser	p.Pro51Ser	p.Pro51Ser	p.Pro51Ser	p.Pro51Ser	p.Pro51Ser	p.Pro51Ser
OKR gain	0.90	0.87	0.94	—	0.91	—	—	—
COR gain	0.83	—	0.92	—	—			

	Patient 9	*Patient 10*	*Patient 11*	*Patient 12*	*Patient 13*	*Patient 14*	*Patient 15*	*Patient 16*
Otolith tests								
Age	58	60	63	54	57	77	69	74
4 cm off-axis rotation	—	—	—	—	—	—	—	—
oVEMP	—	—	—	—	—	—	—	—
cVEMP	—	—	—	—	—	—	—	—
OCR video	—	—	—	—	—	—	—	—
Canal tests								
Video head impulse test	Catch-up saccades (no VOR)	Catch-up saccades (no VOR)	Catch-up saccades (no VOR)	Catch-up saccades (no VOR)	Catch-up saccades (no VOR)	—	—	—
VOR (90°) step test	No postrotary nystagmus	No postrotary nystagmus	No postrotary nystagmus	—	No postrotary nystagmus	No postrotary nystagmus	No postrotary nystagmus	No postrotary nystagmus
VOR (250°) step test	—	—	—	—	—	—	—	—
Caloric test (30 and 44°C)	No reactive eye movements	No reactive eye movements	No reactive eye movements	—	No reactive eye movements	No reactive eye movements	No reactive eye movements	No reactive eye movements
Other tests								
DNA testing	p.Pro51Ser	p.Pro51Ser	p.Pro51Ser	p.Pro51Ser	p.Pro51Ser	p.Pro51Ser	p.Pro51Ser	p.Pro51Ser
OKR gain	0.85	0.92	0.81	—	0.87	—	—	—
COR gain	—	—	—	—	—	—	—	—

Off-axis rotation, eccentric (off-center) rotation such that center of head is away from axis of rotation; no otolithic function, no ocular counterroll. oVEMP, ocular vestibular evoked myogenic potential measured underneath the eyes; no response means no systematic effect in repeated testing. cVEMP, cervical vestibular evoked myogenic potential measured at the sternocleidomastoid muscle (air conducted and bone conducted). OCR video, video recording of eye movements during ocular counterroll (OCR). VOR, vestibuloocular reflex initiated by velocity step tests. OKR gain, optokinetic reflex: measuring the response gains of the eyes during optokinetic stimulation; stimulus velocity 40°/s. COR gain, cervical ocular reflex: measuring the response gain (eye velocity/body velocity) during body under head rotation (amplitude 30°, f = 0.1 Hz). —, Test was not performed in the patient.

of induced reactive eye movements during caloric tests, which were performed with 30-s irrigation with 150–200 cm^3 of water at 30°C and 44°C sequentially. We also performed the head impulse test (Weber et al. 2008), which showed no catch-up saccades after head rotation as a sign of semicircular canal paresis. In addition to testing the vestibular system directly, the present study also reports increases in optokinetic response gain and cervical ocular reflex gain in the patients who underwent these tests, both indicative of compensatory mechanisms for complete vestibular loss (Huygen et al. 1989, 1991; Huygen and Verhagen 2011).

Setup. Subjects were seated in a chair in front of an OLED TV screen (LG 55EA8809, 123 cm × 69 cm, 1,920 × 1,080 pixels, refresh rate 60 Hz) and were asked to position the head in one of three predefined roll orientations (termed upright and 15° or 30° right-ear-down head tilt conditions). An adjustable head cushion was used to support the roll-tilt of the head while the body remained upright. Head-in-space orientation was monitored several times per session with a digital angle meter. Experiments took place in complete darkness. Subjects were seated 95 cm in front of the screen, and the frame and rod were presented with a luminance of 0.23 cd/m^2. Subjects' responses were recorded with a button box.

Experimental procedure. Figure 1*A* provides a schematic illustration of the task. Stimuli were presented in gray on a black background. Each trial started by presentation of a square frame of 18.3 × 18.3° visual angle (31.5 × 31.5 cm), with a line width of 0.2° visual angle. The orientation of the displayed frame was randomly chosen from a set of 18 angles between −45° and +40° in intervals of 5°. After 250 ms, a luminous rod (angular subtense 12.6° and width 0.2°) was briefly flashed for 33 ms (i.e., 2 frames) in the center of the frame. The rod orientation was randomly selected from a set of nine condition-specific rod orientations (upright: −12°, −8°, −5°, −2°, 0, 2°, 5°, 8°, and 12°; 15° and 30° head tilt: −15°, −10°, −5°, −2°, 0, 2°, 5°, 10°, and 15°) centered on the separately measured subjective visual vertical (dark SVV, see below). We chose to extend this range in the 15° and 30° head-tilt conditions because previous experiments (including our own) have shown that subjects become more variable with larger head tilts (Alberts et al. 2015; Clemens et al. 2011; Tarnutzer et al. 2010). Subjects indicated whether they perceived the orientation of the rod as rotated clockwise or counterclockwise from the gravitational vertical by pressing the right or left button of a button box, respectively. Subjects were asked to respond as fast as possible. After the response, the frame disappeared and the screen turned black for 500 ms before the next trial started. Combinations of frame and rod orientation were presented pseudorandomly, with each set containing one repetition of each combination. In total, 10 sets were tested, yielding 1,620 trials per condition, i.e., per head orientation.

Preceding this experimental procedure, the perceived orientation of upright in the absence of the frame, the dark SVV, was measured in all three head-tilt conditions. Subjects were presented with 10 sets of nine randomly ordered rod orientations (−12°, −8°, −5°, −2°, 0, 2°, 5°, 8°, and 12°) centered on the true gravitational vertical, yielding a total of 90 trials. In each trial, subjects had to indicate whether the orientation of the rod was rotated clockwise or counterclockwise from the gravitational vertical by pressing the right or left button of a button box, respectively. We also estimated the dark SVV by looking at the orientation at which the subject responded 50% left and 50% right. We used this dark SVV as the orientation relative to which the condition-specific rod orientations were presented in the actual rod-and-frame tasks, described above.

Psychophysical analysis. Clockwise frame and rod orientations were defined as positive. For each frame orientation, the proportion of clockwise responses as a function of rod orientation was computed. A psychometric curve was fitted through these proportions with a cumulative Gaussian function in MATLAB (Wichmann and Hill 2001):

$$P(\mathrm{CW}) = \lambda + (1 - 2\lambda)\frac{1}{\sigma\sqrt{2\pi}}\int_{-\infty}^{x} e^{-(y-\mu)^2/2\sigma^2}\mathrm{d}y \qquad (1)$$

in which x represents the rod orientation in space and λ the lapse rate, accounting for individual stimulus-independent errors. The mean μ of the Gaussian and the standard deviation σ of the Gaussian account for subjects' perceived orientation of gravity (i.e., the bias) and response variability, respectively. Fits were performed adopting the method of maximum likelihood estimation using the MATLAB routine "fminsearch."

Sensory integration model. To provide a theoretical framework that can explain the observed bias and variability of the perceived gravity direction in the three conditions, we used a Bayesian multisensory integration model to explain the individual responses of the subject (Alberts et al. 2016). Here this model is fit to the subject's response

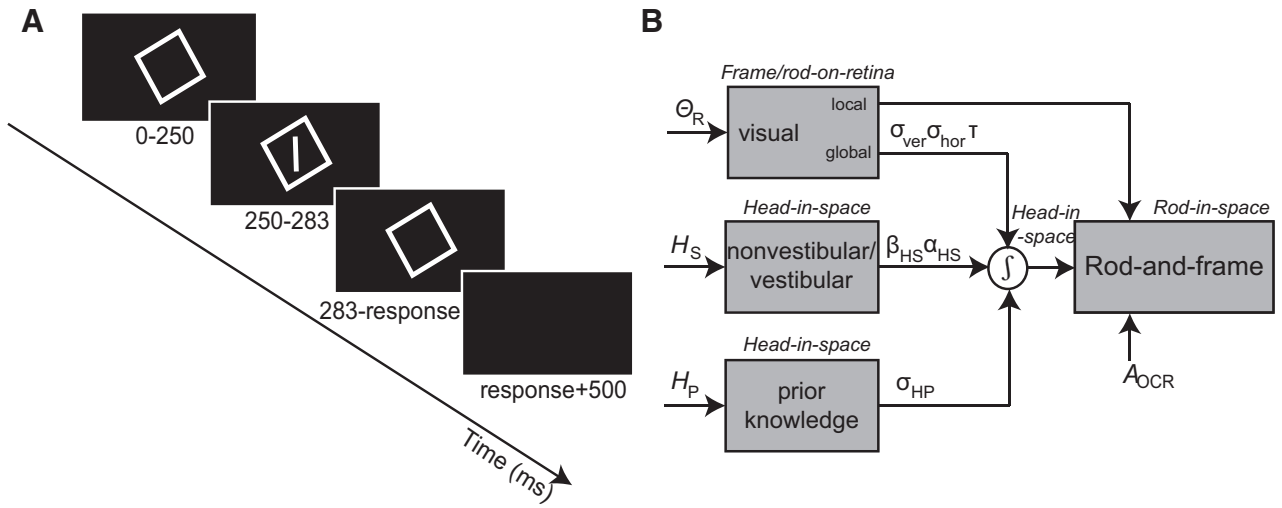

Fig. 1. *A*: experimental procedure of the rod-and-frame task. After presentation of a square frame for 250 ms, a rod is briefly (33 ms) flashed within the frame. When the rod disappears, the square remains visible until the subject responds as to whether the rod was rotated CW or CCW from upright. A 500-ms black screen is presented before the start of a new trial. *B*: schematic representation of the Bayesian model for verticality perception. For an optimal estimate of head-in-space orientation, used in the rod-and-frame task, the model integrates the global visual context (θ_R) together with vestibular/nonvestibular information (H_S) and prior information (H_P) that the head is usually upright. Sensory signals are assumed to be accurate but contaminated with noise (visual: σ_{ver}, σ_{hor}; vestibular/nonvestibular: α_{HS}, β_{HS}; prior: σ_{HP}). The perceived orientation of the rod in space is then obtained by coordinate transforming the optimal estimate of head-in-space orientation with the eye-in-head orientation (uncompensated ocular counterroll, A_{OCR}) and the line-on-eye orientation (assumed to be veridical).

data to reverse engineer the noise properties of the sensory signals and quantify the reweighting of visual and nonvestibular cues at the individual patient level.

Figure 1*B* shows a schematic representation of the model, specifying optimal integration of visual, vestibular, and/or nonvestibular and prior knowledge information about head-in-space orientation. We first describe how the model works in the absence of visual contextual cues. To provide an estimate of head-in-space orientation, the brain can rely on vestibular information (only healthy control subjects) and nonvestibular information (patients and healthy control subjects), such as neck proprioceptive signals (Fig. 1*B*). Following our previous work (Alberts et al. 2016; Clemens et al. 2011), we assumed that the head-in-space signal (H_S) provided by the vestibular and/or nonvestibular sensors is accurate but contaminated with noise. The magnitude of this noise (σ_{HS}) increases linearly with roll-tilt angle and is described as

$$\sigma_{HS} = \alpha_{HS}\left|H_S\right| + \beta_{HS} \quad (2)$$

in which β_{HS} is the noise level when seated upright and α_{HS} the proportional increase of the noise level with tilt angle H_S. In addition to vestibular and/or nonvestibular head-in-space information, the model further assumes that the brain uses prior experience that the head is most often upright (Clemens et al. 2011; De Vrijer et al. 2008; Eggert 1998; MacNeilage et al. 2007; Vingerhoets et al. 2009). This is modeled by a Gaussian prior centered at 0° head-in-space orientation, with standard deviation σ_{HP}.

To explain rod-and-frame effects, the model needs a stage to incorporate visual information. This can be either local (the orientation of the rod and the frame) or global (frame-induced head-in-space orientation) visual information. Noise on the local visual information is assumed to be negligible compared with the other sources. As to the global visual information, the model assumes that contextual cues are mainly extracted from the four cardinal directions of the frame (Vingerhoets et al. 2009). While in Vingerhoets et al. (2009) we assumed equal noise levels for the horizontal and vertical frame cues, in Alberts et al. (2016) we assumed and confirmed nonequal contributions of the cardinal axes based on the finding that the peak influence of the frame is biased to the vertical cardinal direction. This contextual information is modeled as a sum of four von Mises distributions, with one peak at the true frame orientation in retinal coordinates (θ_R) and the other peaks at 90° intervals:

$$P\left(\hat{\theta}_R \middle| H_S\right) = \sum_{i=1}^{4} \frac{\exp\left\{\kappa(i) \times \cos\left[\theta_R + \varphi(i) - H_S\right]\right\}}{2\pi \times I_0\left[\kappa(i)\right]} \quad (3)$$

in which 2π is a normalization factor, φ denotes the four different cardinal directions of the frame (0°, 90°, 180°, 270°), κ is the concentration parameter, and I_0 is the modified Bessel function of the first kind with order zero. The concentration parameter κ ($\kappa \approx 1/\sigma^2$) of the four von Mises distributions is inversely related to the noise of the vertical (σ^2_{ver}) and horizontal (σ^2_{hor}) cardinal directions and depends on the rate of increase/decrease of these noise levels (τ) with rotation of the frame.

$$\kappa(i) = \left[\kappa_1, \kappa_2, \kappa_1, \kappa_2\right] \quad (4)$$

$$\kappa_1 = \kappa_{ver} - \left[1 - \cos\left(\left|2 \times \theta_R\right|\right)\right] \times \tau \times \left(\kappa_{ver} - \kappa_{hor}\right) \quad (5)$$

$$\kappa_2 = \kappa_{hor} + \left[1 - \cos\left(\left|2 \times \theta_R\right|\right)\right] \times \left(1 - \tau\right) \times \left(\kappa_{ver} - \kappa_{hor}\right) \quad (6)$$

The rate at which κ_1 decreases and κ_2 increases is determined by decline parameter τ, which ranges between 0 and 1. The horizontal and vertical components of this contextual prior are indistinguishable at 45° ($\theta_R = 45°$), and therefore κ_1 and κ_2 become the same.

To estimate the head-in-space orientation, the model uses Bayes' rule to integrate optimally visual contextual information with prior knowledge and nonvestibular/vestibular information. The head-in-space orientation follows from the mean of the posterior distribution. The perceived orientation of the rod in space is then obtained by correcting for the eye-in-head position (uncompensated ocular counterroll, A_{OCR}). For a more detailed description of the mathematics, including the Bayesian optimal integration, we refer the reader to Alberts et al. (2016).

Model fitting. The above model contains eight free parameters (α_{HS}, β_{HS}, σ_{HP}, A_{OCR}, κ_{ver}, κ_{hor}, τ, and a lapse rate λ) that were estimated simultaneously based on responses from all three conditions (see Alberts et al. 2016 for details on our fitting procedure). While the model was optimized based on the concentration parameters, for convenience we also converted them to sigmas (σ_{ver} and σ_{hor}), which are easier to interpret ($\kappa \approx 1/\sigma^2$). Note that a single lapse rate, λ, was incorporated to account for lapses in the responses of the subject. In total, the eight free parameters had to be reverse engineered from 4,860 stimuli and responses (3 conditions × 18 frame orientations × 9 line orientations × 10 repetitions). We fitted the model by maximizing the likelihood of the data in relation to these free parameters. Optimal parameters were obtained by minimizing the negative likelihood function with the MATLAB routine "fmincon" (Alberts et al. 2016; Clemens et al. 2011). This optimization routine imposes constraints on the parameter values, keeping them in a behaviorally and physiologically realistic range (see Table 2). This routine was repeated three times with different initial starting values to make sure that the minimization procedure found a global minimum rather than a local minimum. Standard deviations of the fitted parameter values were obtained by performing 100 bootstrap runs. For each run, 4,860 stimuli (reflecting the size of the data set) and responses were randomly sampled with replacement from the raw data, keeping the number of trials from each condition equal. Sensory weights were computed with estimates of the sensory and prior variability.

Statistics. All analyses were performed off-line with MATLAB and SPSS. We performed *t*-tests to test for differences in parameter values between groups. A two-way paired univariate analysis of variance (ANOVA) with subject as a random factor was used to compare the effect of group (patients vs. control subjects) and orientation (upright, 15° or 30° head tilt) on sensory weight.

RESULTS

Psychometric results. Figure 2*A* shows the proportion of clockwise (CW) responses in the upright condition plotted against each rod orientation for three exemplar frame orientations [20° counterclockwise (CCW), upright, and 20°CW] in a representative patient and an age-matched healthy control subject. When the frame is displayed upright (Fig. 2*A*, *center*), both the patient and the healthy control subject show high probabilities of CW responses for large CW rod orientations (positive angles) and low probabilities of CW responses for large CCW rod orientations (negative angles). Around a rod orientation of 0° their responses are near chance level, suggesting they are virtually unbiased. The response variability, i.e., the range of rod orientations over which they transition from CCW to CW responses, seems larger for the patient than for the control subject. We fit psychometric curves to quantify the bias and response variability.

Indeed, psychometric curves of both the patient and the healthy control subject show near-zero biases when the frame is upright (see dashed lines at crossing 50% CW response and psychometric curve in Fig. 2*A*; patient: $\mu = -0.9°$, control subject: $\mu = 0.2°$). The psychometric curves also confirm that response variability, reflected by the steepness of the curve, is higher for the patient than for the control subject (patient: $\sigma = 3.6°$, control subject: $\sigma = 1.0°$).

When the frame is rotated to ±20° (Fig. 2*A*, *left* and *right*), both the patient and the control subject perceive the gravitational vertical shifted in the direction of the frame orientation.

Table 2. *Best-fit parameter values including bootstrapped SD for each individual patient and control subject*

	β_{HS}	α_{HS}	σ_{ver}	σ_{hor}	τ	σ_{HP}	λ	R^2
Patients								
P1	5.33 ± 0.31	0.18 ± 0.01	6.70 ± 0.44	129.77 ± 48.52	0.77 ± 0.03	>30	0.06 ± 0.02	0.53
P2	4.32 ± 0.29	0.11 ± 0.02	4.32 ± 0.84	33.30 ± 2.87	0.92 ± 0.05	>30	0.01 ± 0.01	0.58
P3	7.89 ± 0.20	0.00 ± n.a.	1.19 ± 0.48	>250	0.99 ± 0.00	10.17 ± 0.29	0.04 ± 0.01	0.67
P4	9.69 ± 0.54	0.05 ± 0.03	7.62 ± 0.51	44.17 ± 4.99	0.79 ± 0.04	13.25 ± 0.81	0.02 ± 0.01	0.64
P5	>15	0.24 ± 0.05	5.29 ± 1.17	27.31 ± 14.61	0.84 ± 0.06	>30	0.02 ± 0.01	0.64
P6	8.29 ± 0.49	0.30 ± 0.03	3.67 ± 0.38	53.03 ± 10.51	0.82 ± 0.02	20.54 ± 1.83	0.00 ± 0.00	0.70
P7	2.51 ± 0.17	0.36 ± 0.02	5.34 ± 0.89	>250	0.87 ± 0.03	15.76 ± 0.82	0.05 ± 0.01	0.74
P8	6.29 ± 0.31	0.13 ± 0.02	4.74 ± 0.32	37.34 ± 3.50	0.84 ± 0.02	>30	0.01 ± 0.01	0.76
P9	2.46 ± 0.10	0.22 ± 0.02	1.44 ± 0.74	144.02 ± 38.17	0.99 ± 0.01	14.42 ± 1.04	0.01 ± 0.00	0.65
P10	3.54 ± 0.16	0.12 ± 0.01	4.38 ± 0.72	211.89 ± 59.59	0.95 ± 0.02	10.28 ± 0.69	0.01 ± 0.01	0.80
P11	4.64 ± 0.25	0.25 ± 0.01	9.32 ± 1.16	>250	0.77 ± 0.12	19.21 ± 3.15	0.07 ± 0.02	0.42
P12	2.13 ± 0.13	0.19 ± 0.01	1.40 ± 0.52	>250	0.67 ± 0.03	>30	0.14 ± 0.01	0.80
P13	5.03 ± 0.21	0.00 ± n.a.	4.50 ± 0.97	25.30 ± 2.99	1.00 ± n.a.	4.92 ± 0.21	0.00 ± 0.00	0.81
P14	>15	0.00 ± n.a.	7.26 ± 0.50	25.55 ± 3.25	1.00 ± n.a.	10.84 ± 0.57	0.33 ± 0.02	0.39
P15	12.63 ± 1.00	0.14 ± 0.06	8.21 ± 0.69	35.21 ± 3.67	0.93 ± 0.03	28.61 ± 1.13	0.00 ± n.a.	0.75
P16	8.12 ± 0.52	0.35 ± 0.04	4.48 ± 0.39	43.19 ± 6.61	0.78 ± 0.02	>30	0.01 ± 0.00	0.74
Mean ± SD	5.92 ± 3.07	0.20 ± 0.10	4.99 ± 2.41	67.51 ± 60.45	0.87 ± 0.10	14.80 ± 6.68	0.05 ± 0.08	0.66 ± 0.13
Control subjects								
C1	10.38 ± 0.53	0.00 ± n.a.	7.20 ± 0.51	27.49 ± 2.62	1.00 ± 0.01	11.76 ± 0.73	0.07 ± 0.02	0.75
C2	6.11 ± 0.31	0.10 ± 0.02	10.78 ± 0.74	33.66 ± 4.73	0.96 ± 0.04	>30	0.03 ± 0.01	0.54
C3	5.31 ± 0.13	0.33 ± 0.02	6.68 ± 1.39	51.23 ± 11.95	1.00 ± 0.01	22.11 ± 1.39	0.00 ± 0.00	0.72
C4	4.07 ± 0.22	0.09 ± 0.01	6.80 ± 0.62	41.26 ± 5.83	0.81 ± 0.06	21.53 ± 1.78	0.01 ± 0.00	0.81
C5	4.72 ± 0.20	0.00 ± n.a.	7.76 ± 0.92	43.51 ± 24.31	1.00 ± n.a.	6.61 ± 0.34	0.01 ± 0.00	0.59
C6	6.95 ± 0.14	0.00 ± n.a.	17.58 ± 1.18	53.10 ± 4.35	1.00 ± n.a.	13.08 ± 0.46	0.00 ± 0.00	0.05
C7	5.12 ± 0.24	0.21 ± 0.04	8.15 ± 1.06	40.39 ± 15.45	0.99 ± 0.02	18.94 ± 2.97	0.01 ± 0.01	0.69
C8	7.65 ± 0.41	0.04 ± 0.02	6.58 ± 0.32	24.83 ± 1.83	0.95 ± 0.04	9.22 ± 0.49	0.01 ± 0.01	0.89
C9	3.21 ± 0.17	0.05 ± 0.01	6.03 ± 2.22	32.04 ± 14.66	0.98 ± 0.04	8.47 ± 0.81	0.02 ± 0.01	0.58
C10	5.08 ± 0.25	0.12 ± 0.02	4.35 ± 0.44	44.70 ± 5.68	0.96 ± 0.01	12.61 ± 0.67	0.00 ± 0.00	0.60
C11	4.78 ± 0.19	0.10 ± 0.01	7.72 ± 1.16	36.97 ± 8.68	0.98 ± 0.02	18.75 ± 1.03	0.00 ± n.a.	0.66
C12	5.57 ± 0.29	0.00 ± n.a.	10.59 ± 0.83	51.90 ± 26.79	1.00 ± n.a.	7.17 ± 0.39	0.04 ± 0.01	0.58
C13	6.17 ± 0.29	0.03 ± 0.02	7.44 ± 0.56	21.01 ± 1.61	1.00 ± n.a.	8.21 ± 0.59	0.03 ± 0.01	0.60
C14	4.44 ± 0.17	0.23 ± 0.02	6.68 ± 0.54	39.55 ± 11.00	0.86 ± 0.03	16.83 ± 0.75	0.00 ± 0.00	0.76
C15	3.75 ± 0.17	0.11 ± 0.01	5.14 ± 1.91	46.49 ± 12.42	0.99 ± 0.03	12.80 ± 0.79	0.00 ± 0.00	0.53
C16	8.75 ± 0.33	0.00 ± n.a.	9.96 ± 0.55	40.41 ± 4.72	1.00 ± n.a.	11.43 ± 0.59	0.05 ± 0.01	0.30
Mean ± SD	5.75 ± 1.89	0.12 ± 0.09	8.09 ± 3.09	39.28 ± 9.56	0.97 ± 0.06	13.30 ± 5.17	0.02 ± 0.02	0.60 ± 0.20

R^2 is a measure for the goodness of fit of the model. > means that the parameter value was capped at the upper limit. n.a., Not available.

This bias is larger for the patient ($\mu = -10.9°$ and $\mu = 5.5°$) compared with the control subject ($\mu = -2.0°$ and $\mu = 1.5°$), reflecting the increased reliance on visual context as indicator of upright by the patient. Note that the slope of the psychometric curves decreases with larger frame orientation in both the patient and the control subject, which means that their response variability has increased compared with upright.

Figure 2, *B* and *C*, shows the psychometrically assessed biases (Fig. 2*B*) and variabilities (Fig. 2*C*) for all frame orientations in the representative patient and control subject, for all three head-tilt conditions. The patient's and control subject's bias patterns show the shift of perceived gravitational vertical in the direction of the frame for intermediate frame orientations, but this shift is much larger for the patient. Also note that the patient's bias pattern does not change much when the head is tilted, whereas the control subject shows an increased magnitude of the pattern. Furthermore, the patient's response variability is lowest when the frame is upright and increases for larger frame orientations, in all three conditions. This increase of variability with frame orientation seems larger for the larger head tilts. The variability of the control subject is much smaller than that of the patient, and the variability pattern changes with head tilt angle.

Bayesian optimal integration model. The solid lines in Fig. 2, *B* and *C*, represent the predicted biases and variabilities of the Bayesian optimal integration model after fitting it to the behavioral responses in all conditions simultaneously. In both the patient and the healthy control subject, the model captures bias and variability patterns quite well. Best-fit parameter values and their bootstrapped standard deviations (±SD) are listed in Table 2 (*participants P15* and *C15*). Of note, the model also predicts unwarranted kinks in the biases for the 15° and 30° tilt conditions, at frame orientations −35° and −20°, respectively. Mathematically, these unrealistic kinks arise because of the transition of the contextual prior induced by the frame at 45° frame angles (in head coordinates) and its interaction with the upright prior.

Figure 3 shows mean bias (Fig. 3*A*) and variability (Fig. 3*B*) as a function of frame orientation across the group of patients ($n = 16$) and the group of healthy control subjects ($n = 16$). The mean data, including the standard deviation across subjects, resemble the data of the representative subjects in Fig. 2, *B* and *C*. The mean prediction of the Bayesian optimal integration model is shown by the solid lines in Fig. 3, with the shaded areas indicating the standard error across subjects. The model captures the bias data of both groups. The model also accounts for the increase in variability with larger frame orientations, as well as the increase with head tilt. The best-fit parameters and their bootstrapped SD values that are reverse engineered by fitting the model are shown in Table 2. Table 2

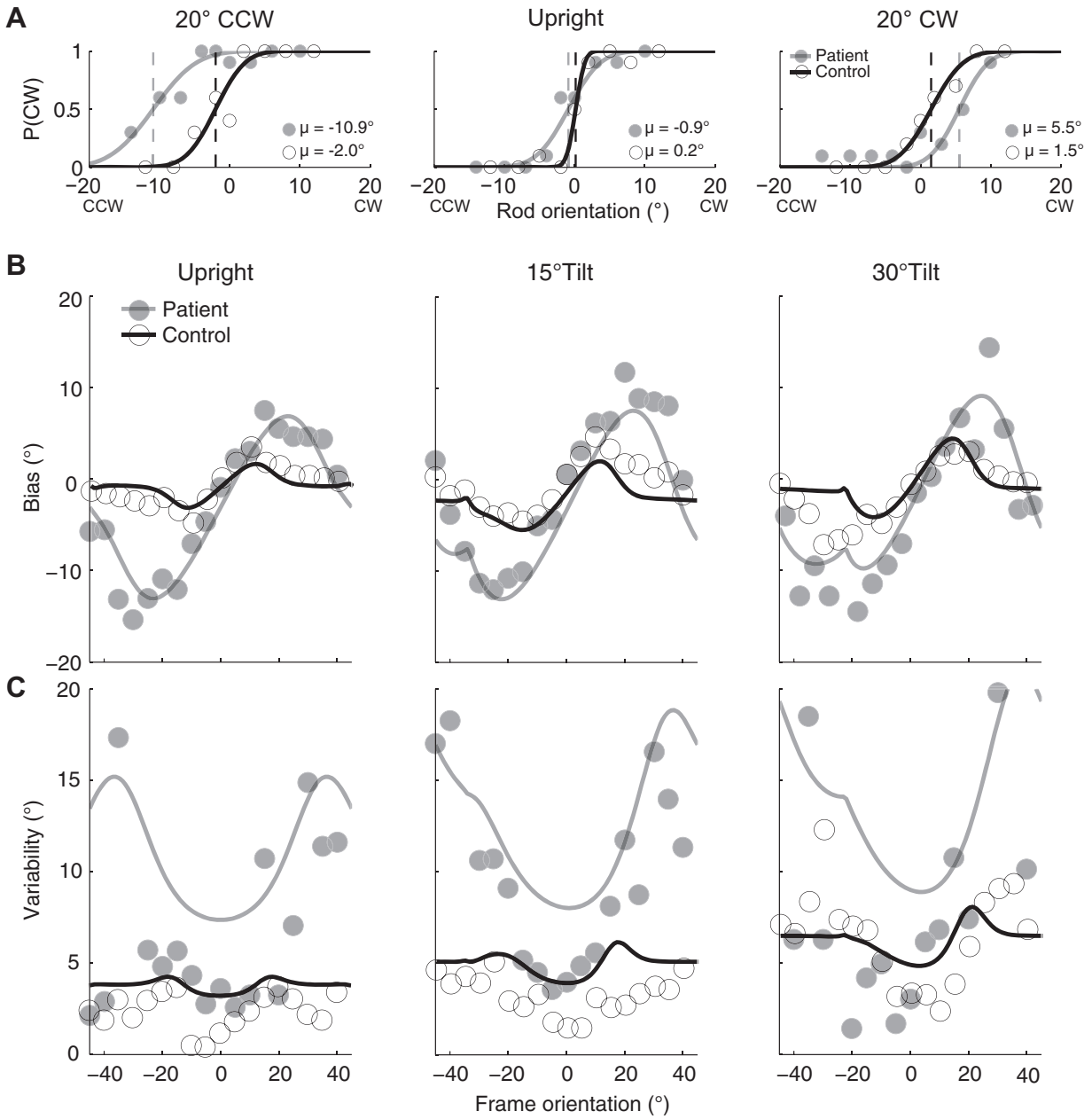

Fig. 2. *A*: probability of CW responses plotted against rod orientation for 3 exemplar frame orientations (20° CCW, upright, and 20° CW) in a representative bilateral vestibular areflexic patient (filled circles) and an age- and sex-matched healthy control subject (open circles). In each panel, the solid lines plotted through the data represent the psychometric functions, quantifying the bias (μ, dashed line) and response variability of the subject. *B* and *C*: bias and response variability with frame orientation for the representative patient and control subject in *A* for all 3 head-in-space orientations. Solid lines plotted through the data represent the best fit of the Bayesian optimal integration model, fitted to all responses simultaneously. Best-fit parameters are found in Table 2 (*participants P15*, *C15*).

also lists R^2 values as a measure of how much of the variability in the data is actually explained by the model. These values were very similar for patients (mean: 0.66 ± 0.13) and control subjects (0.60 ± 0.20).

Inferred sensory signal properties. The model-based psychometric predictions shown in Fig. 3 are derived from the reverse-engineered parameters describing the properties of the underlying sensory systems (Table 2). Parameter β_{HS} reflects the noise in the nonvestibular/vestibular sensors when the head is upright, and α_{HS} represents the linear change of this noise with tilt angle. In patients, β_{HS} ranges between 2.1° and 12.6° (excluding the upper limit values) and obviously only reflects a nonvestibular signal, i.e., neck proprioceptive noise. In healthy control subjects, β_{HS} ranges from 3.2° to 10.4°. The values for β_{HS} are not significantly different between the patients and their controls ($P = 0.31$), showing that the patients' neck proprioceptive signal does not differ in precision from the combined precision of the vestibular and neck proprioceptive signal in control subjects. The tilt dependence of the nonvestibular/vestibular noise, signified by α_{HS}, is significantly positive for both patients ($P < 0.001$) and healthy control subjects ($P = 0.002$) and does not differ between the two groups ($P = 0.11$), so despite the absence of vestibular input for the vestibular areflexic patients, the noise characteristics of nonvestibular signals in patients cannot be dissociated from the noise characteristics of the integrated vestibular and nonvestibular signals in healthy

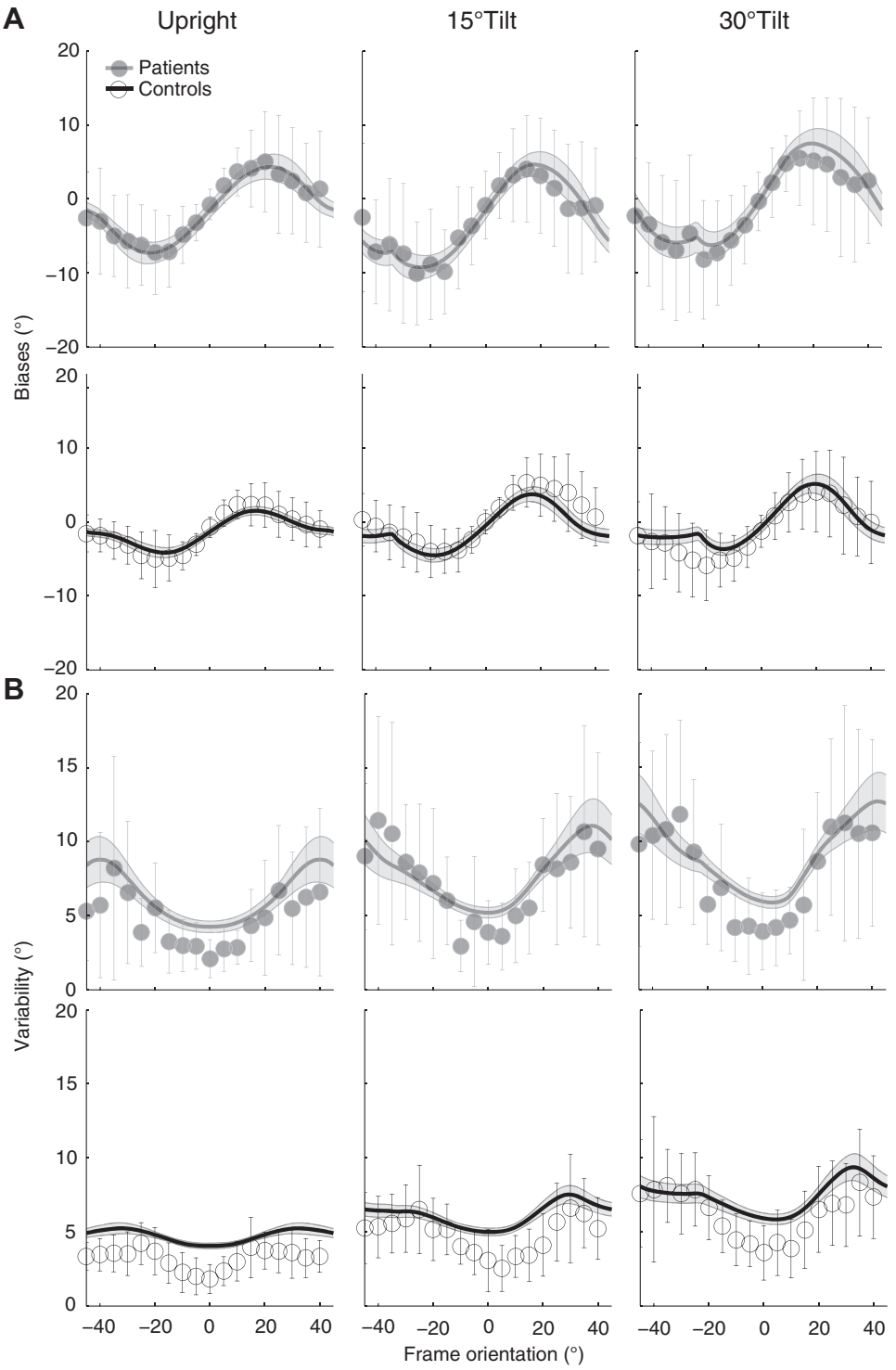

Fig. 3. Mean bias (*A*) and response variability (*B*) plots across all patients ($n = 16$) and control subjects ($n = 16$). Error bars on the data represent the standard deviation across subjects. Solid lines through the data show the mean best fit across all patients and control subjects, with the shaded areas indicating the standard error on the model best fits.

control subjects. This means that the differences in variability between patients and control subjects, as shown in Figs. 2 and 3, are a reflection of how these signals are integrated with visual context, which differs between the two groups, as we describe below.

The visual contextual information of the frame, used as an indicator of upright, is captured by three parameters in the model. In Table 2, we list the standard deviations of the vertical and horizontal von Mises distributions ($\sigma^2 \approx 1/\kappa$) for the upright frame, captured by the vertical and horizontal noise levels, σ_{ver} and σ_{hor}, respectively. Parameter τ determines how these noise levels change with increasing tilt angle of the frame, σ_{ver} and σ_{hor} being equal for 45° frame tilt angle. In both groups, the noise in the vertical direction (σ_{ver}) is smaller than that in the horizontal direction (σ_{hor}, $P < 0.001$); hence subjects base their visually based percept of verticality mainly on the vertical orientation of the frame. Interestingly, patients show a significantly narrower prior (smaller width) on the vertical context direction than healthy control subjects (Fig. 4 and Table 2; $P = 0.01$), suggesting they have a stronger reliance on vertical context being informative for

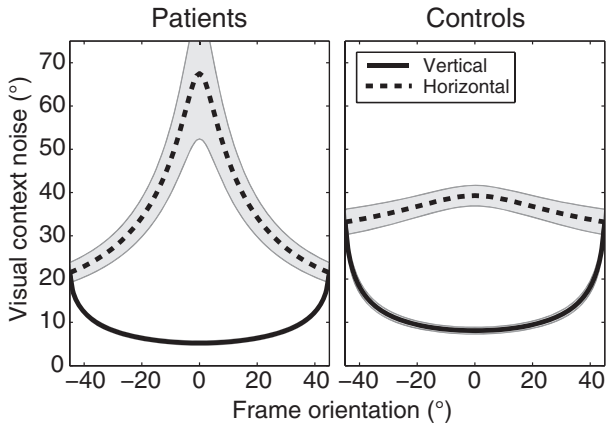

Fig. 4. Mean vertical (σ_{ver}) and horizontal (σ_{hor}) visual context noise across subjects (patients, $n = 16$; control subjects, $n = 16$) plotted against frame orientation. Shaded areas represent the standard error on the noise parameter values.

gravity perception compared with control subjects. This is further confirmed by a significantly lower decline parameter value (τ, $P = 0.01$) showing that the rate of increase in noise of this vertical contextual cue with frame orientation is lower than in healthy control subjects.

Figure 4 summarizes these effects, showing how the vertical and horizontal contextual prior changes with frame orientation for both groups. Also, note that the noise of horizontal visual context is relatively constant in healthy control subjects, whereas the noise in patients is very high when the frame is upright. Parameter σ_{HP} reflects the uncertainty in the a priori assumption about likely head orientations being around upright in space. This prior has a width $> 4.9°$ and does not differ between patients and control subjects ($P = 0.06$). Finally, the lapse rate (λ) is small and does not differ between the groups ($P = 0.16$).

Sensory weights. Based on the noise characteristics of the individual sensory modalities, captured by the parameters in Table 2, the sensory weights for vertical visual context, nonvestibular/vestibular, and prior knowledge can be computed in all conditions. Figure 5*A* shows the distribution of these weights for patients (Fig. 5*A*, *top*) and control subjects (Fig. 5*A*, *bottom*), with the shaded areas indicating the standard error across subjects. In both groups, the weight for vertical visual context is highest when the frame is aligned with gravity in the upright condition (Fig. 5*A*, *left*). Because of an increase of uncertainty about the vertical context with larger frame orientations (see model), this contextual weight decreases. Consequently, the weights of prior knowledge and nonvestibular/vestibular signals increase with frame orientation because their

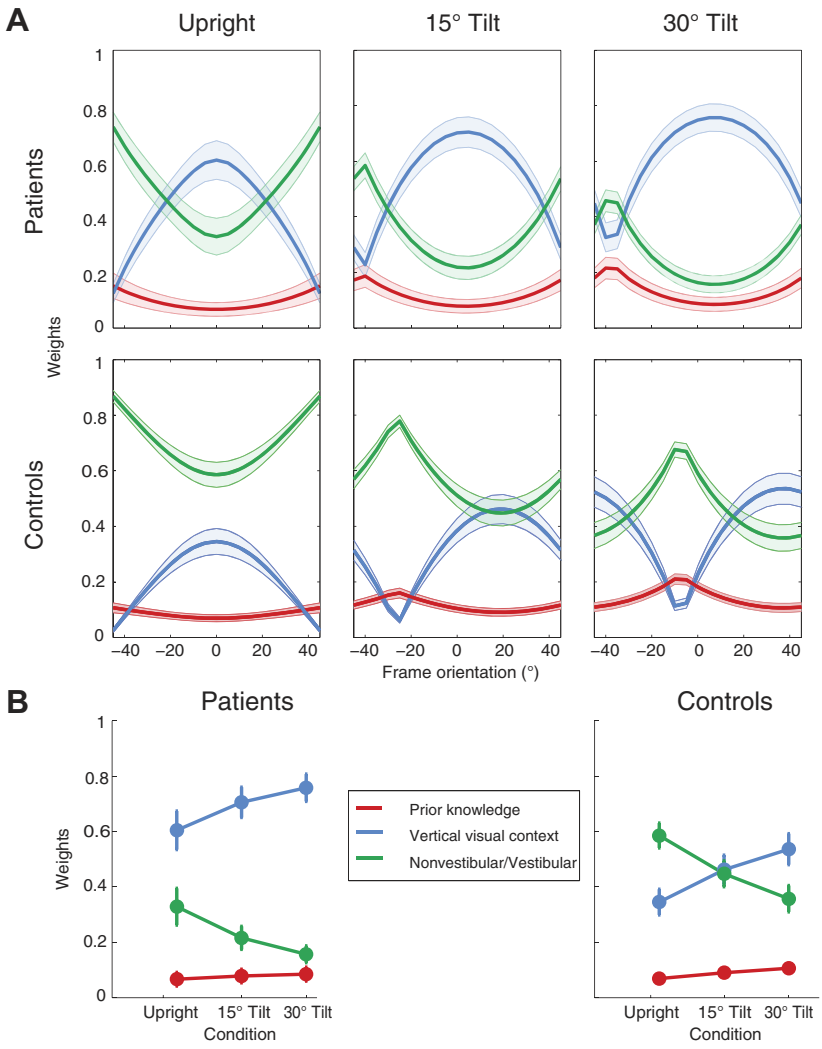

Fig. 5. *A*: mean vertical visual context, nonvestibular/vestibular, and prior weight distributions over frame orientation in all 3 head-in-space orientations for patients ($n = 16$, *top*) and healthy control subjects ($n = 16$, *bottom*). Shaded areas represent the standard error over the mean weights. *B*: distribution of mean vertical visual context, vestibular/nonvestibular, and prior sensory weights in patients (*left*) and control subjects (*right*) at maximum vertical visual weight. Error bars represent the standard error on the distribution of weights across subjects.

noise levels do not depend on frame orientation. When the head is tilted, the weight distribution is shifted along the frame orientation axis. This shift can be explained by a shift in perceived orientation of upright for the dark SVV (i.e., vertical perception without visual context); when the head is roll-tilted in darkness, perception of upright is no longer aligned with the true gravitational vertical. This means that an upright frame is no longer corresponding to the perceived orientation of what is upright in darkness and therefore is not associated with the maximum visual contextual weight.

The difference between the patients and control subjects is most prominent in the visual and nonvestibular weights. Figure 5*B* shows a condensed version of Fig. 5*A*, plotting the modality weights for the 0° frame orientation for the three head tilts. The plot clearly shows a higher visual weight for the patients compared with the control subjects, whereas the nonvestibular weight is smaller in magnitude. The nonvestibular weight decreases with head tilt because the noise levels of the nonvestibular sensory signals increase with tilt angle (α_{HS} is larger than zero), in both patients and control subjects.

Repeated-measures ANOVAs with factors group and tilt angle on the weights of the three sensory signals revealed a significant tilt effect in all three weights [visual context: $F_{(2,14)} = 24.3$, $P = 0.000$; (non)vestibular: $F_{(2,14)} = 28.0$, $P = 0.000$; prior knowledge: $F_{(2,14)} = 15.6$, $P = 0.000$] and a significant group effect in the visual context weight [$F_{(1,15)} = 10.8$, $P = 0.005$] and the (non)vestibular weight [$F_{(1,15)} = 14.1$, $P = 0.002$] but not the prior knowledge weight [$F_{(1,15)} = 0.2$, $P = 0.67$]. There were no significant interaction effects. In conclusion, these results indicate that our patients rely more on visual context than healthy control subjects, despite the fact that their nonvestibular signals show similar noise characteristics as the combined vestibular and nonvestibular signals in the control subjects.

Individual differences. A strength of the reversed Bayesian engineering approach is that the weights can be established at the single-subject level. Figure 6 shows the visual weights as a function of the nonvestibular/vestibular weight in upright individuals. Note that the deviation from the diagonal reflects the weight given to the prior. The average weight across participants is shown with a cross in Fig. 6. Data of most patients (Fig. 6, *left*) lie in the top left part of the graph, indicative of a high visual context weight. However, there are also two patients with a low visual weight and a high nonvestibular weight, hence neck proprioceptive weight. Data of healthy control subjects (Fig. 6, *right*) mostly lie in the bottom right part of the graph, indicative of a high combined vestibular and nonvestibular weight. Since their vestibular signal is still intact, they mainly rely on their internal model of what is upright and are influenced less by visual contextual cues.

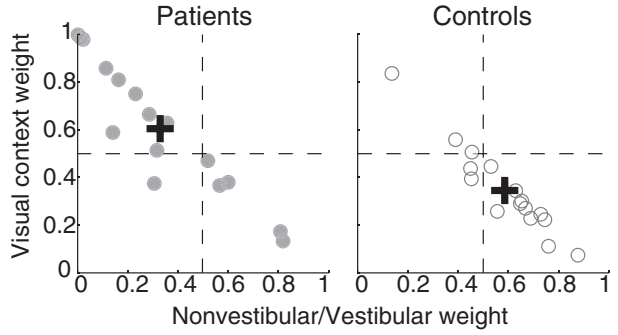

Fig. 6. Individual vertical visual context weights plotted against nonvestibular/vestibular weights in patients ($n = 16$; *left*, filled circles) and control subjects ($n = 16$; *right*, open circles) for an upright frame and an upright seated subject. Crosses represent the mean weights in the upright condition of Fig. 5*B*.

DISCUSSION

Using a rod-and-frame task, we studied sensory processing in a homogeneous group of patients with DFNA9, with severe hearing impairment and vestibular areflexia caused by a mutation in the *COCH* gene. The percept of vertical in these patients shows larger biases in the direction of the visual frame and increased variability compared with a group of age- and sex-matched healthy control subjects. We reverse engineered the noise characteristics of the (remaining) sensory signals, based on optimal Bayesian inference principles, for the individual patients and control subjects. By computing the sensory weights from the individual noise characteristics, we showed that on average patients had a 20–40% increase of the visual weight, confirming the hypothesis that the remaining sensory cues are reweighted after vestibular loss.

Relation to previous work. The present results contribute to an emerging literature suggesting that psychophysical testing can offer insights into peripheral and central vestibular processing not available from standard testing (Lewis 2015). Our approach finds origin in Clemens et al. (2011), in which we estimated the contributions of the various sensory systems in spatial orientation of healthy subjects by testing the perception of both body tilt and the visual vertical. While both tasks require integration of the same sensory signals, their different task constraints impose different interactions between the signals, which was exploited to estimate the sensory contributions to spatial orientation in healthy subjects (see also Guerraz et al. 1998; Tarnutzer et al. 2010). In Clemens et al. (2011) we showed that healthy subjects rely mostly on vestibular signals when upright, reverting to an increased reliance on body somaesthetics for larger tilts, which was attributed to the increased vestibular noise. In Alberts et al. (2015) we used the same two tasks to test spatial orientation in bilateral vestibular patients, suggesting that nonvestibular signals could substitute for vestibular input. To investigate the visual contribution to spatial orientation, we performed the rod-and-frame task under different head and body orientations (Vingerhoets et al. 2009). In that study, we introduced a Bayesian inference model to explain the observed adjustment data, conceiving the visual frame contribution as a distribution of four equally probable head-in-space orientations. This was followed up in Alberts et al. (2016), in which we developed a psychometric version of this task and extended the model with factors to weigh the cardinal frame axes, to account for visual reliability changes, and included uncompensated ocular counterroll (see De Vrijer et al. 2009). Using this model, we showed that subjects flexibly weigh visual panoramic and vestibular information based on their orientation-dependent reliability, explaining the observed verticality biases and the associated response variabilities (Alberts et al. 2016). In the present study, we took this model to demonstrate the reweighting of visual panoramic and nonvestibular information in bilateral vestibular areflexia patients.

Sensory substitution in patients with bilateral vestibular loss. The present psychophysical findings of larger rod-and-frame biases and increased response variabilities for roll-tilted

frames in our patients are in line with previous clinical reports of increased reliance on visual cues in spatial orientation tasks (Bronstein 1999; Bronstein et al. 1996; Cutfield et al. 2014; Dieterich et al. 2007; Grabherr et al. 2011; Guerraz et al. 2001; Lopez et al. 2007). Typically, these studies used adjustment tasks to measure the percept of verticality in the presence of a square frame or a rotating disk, showing that these stimuli have stronger effects on the direction of vertical in patients than in healthy control subjects. Whether this increased visual reliance was due to sensory reweighting could not be established by these studies because of the lack of both a quantitative framework and psychophysical measurements. It is likely that the reweighting of visual and nonvestibular cues in verticality perception is the effect of sensory substitution in the brain, since our group of homogeneous DFNA9 patients show no response in vestibular tests (see Table 1) years after bilateral vestibular areflexia was identified. This idea is confirmed by clinical studies showing sensory substitution in vestibular tasks without visual cues (Alberts et al. 2015; Bronstein and Hood 1986; Cutfield et al. 2014; Gresty et al. 1977; Huygen et al. 1991; Huygen and Verhagen 2011; Kasai and Zee 1978). As monkey studies have shown, this substitution may already arise at the first stages of vestibular processing, the vestibular nuclei, where interaction with visual and somatosensory signals takes place (Cullen 2014; Jamali et al. 2014; Sadeghi et al. 2012).

Therefore the clinically important observation in DFNA9 patients is that they have been able to compensate for the missing vestibular input, i.e., the estimated nonvestibular signal in the patients was of a precision similar to the combined vestibular and nonvestibular signal in the controls. While these similarities may have been accomplished through sensory substitution, our reverse engineering approach further revealed an enhanced reliance on the vertical visual contextual cues (see Table 2), which increases at a lower rate with frame orientations than in healthy control subjects (as indicated by parameter τ in the model). This is another novel observation with clinical relevance that could only be inferred with our computational approach. Of course, this increased reliance on vision by the patients, as indicator of what is upright, causes a larger bias when the cardinal directions of the frame are no longer aligned with the gravitational vertical. In natural conditions, however, visual contextual cues are mainly aligned with the true vertical or horizontal direction (Coppola et al. 1998; Girshick et al. 2011; van der Schaaf and van Hateren 1996; Wei and Stocker 2015), so a smart compensation strategy may rely on these cues, to also serve in many other tasks that involve balance control.

Neurophysiological implications. The idea of sensory reweighting has been widely established in behavioral tasks, but few studies have looked at visual-vestibular reweighting in the brain. Behavioral studies have suggested that the visual-vestibular interactions in the rod-and-frame task are the result of visual contextual information being interpreted as a head-in-space orientation signal, which is combined with a vestibular head-in-space signal to provide a percept of the gravitational vertical (Li and Matin 2005a, 2005b; Matin and Li 1995; Vingerhoets et al. 2009). At the neurophysiological level, Laurens et al. (2016) reported gravity orientation tuning in the thalamus, which may be involved in some of this processing. The parieto-insular cortex, which receives projections from the thalamus, has been implicated in vestibular-based perception of verticality (Brandt and Dieterich 1999). Recent imaging and TMS studies have identified the right superior parietal lobule for the integration of visual contextual information in the perceived gravity reference frame, mediated by reciprocal inhibitory connections between the early visual areas and the right temporal parietal junction (Fiori et al. 2015; Lester and Dassonville 2014; Walter and Dassonville 2008). The latter suggests that if the internal representation of the gravitational vertical (based on vestibular and nonvestibular cues) is less reliable, this will reduce the inhibition of the visual contextual representation. As a result, visual contextual information drives the right superior parietal lobule more strongly in patients compared with healthy control subjects. Here we propose a possible computational mechanism underlying the existing behavioral and neurophysiological data, by showing that our Bayesian optimal integration model is able to explain visual-vestibular interactions in the rod-and-frame task in both patients and control subjects.

Implications for vestibular rehabilitation. Symptoms of vestibular decline are initially reduced based on a process called vestibular adaptation (Cullen et al. 2009; Curthoys 2000; Kitahara et al. 1998; Tjernström et al. 2016) in which, for example, asymmetries in vestibular activity are compensated by cerebellar modulations. However, vestibular function is not restored, and sensory reweighting (or substitution when the sense is completely lost) is needed to reoptimize verticality perception. Often, this process of reweighting (or substitution) is suboptimal and vestibular rehabilitation programs that promote these mechanisms are needed. They focus on recognizing and training the use of other senses to resolve debilitating symptoms after the loss of vestibular functioning (Deveze et al. 2014; Hillier and McDonnell 2011; McCall and Yates 2011).

To further optimize the rehabilitation process, it is important to correctly assess the remaining sensory functioning and the weighting of the different sensors at an individual subject level. Several randomized, prospective studies have documented that vestibular exercises improve postural stability and decrease subjective complaints of dizziness in patients with acute or chronic vestibular hypofunction (McDonnell and Hillier 2015). Vestibular exercises improve visual acuity during head movements or decrease complaints of oscillopsia in these patients (Herdman et al. 2003). So far, it has remained difficult to measure the specific weighting of sensory cues in a comfortable way. Here we show that the simple rod-and-frame task can serve as an instrument to quantify sensory (re)weighting at the single-subject level (Fig. 6). For actual clinical use of this tool, various aspects need to be optimized, from stimulus design, to data recording, test duration, and data analytics. Yet, if successful, such a tool will be able to track the quality of sensory systems across the life span, addressing the risk factors and signaling when (older) people and patients may be in need of additional care or training programs to keep living an active life. In the same vein, such a tool could be used to evaluate the relative benefits of balance prostheses (Guinand et al. 2016) or other sensory restoration devices.

With an individualized assessment, rehabilitation therapies can be tailored toward specific training programs. For example, for balance training exercises (Herdman 2013), our results suggest that patients with a larger visual weight will benefit more from a training tailored toward using visual context as a replacement for the vestibular signal that provides head orientation in space, whereas patients with low visual weight will benefit more from somatosensory training. This weight distribution could shift over

time, i.e., when the disease progresses. Therefore, on the basis of the present findings, we recommend individualized rehabilitation programs that are based on an assessment of sensory reweighting over time. An additional advantage of this individualized assessment is that rehabilitation programs can be evaluated on their efficiency by quantifying the sensory weighting in combination with performance measures at the start and end of the program.

GRANTS

This work was supported by funding from the European Research Council (EU-ERC 283567) and the Netherlands Organisation for Scientific Research (NWO-VICI: 453-11-001) to W. P. Medendorp.

DISCLOSURES

No conflicts of interest, financial or otherwise, are declared by the authors.

AUTHOR CONTRIBUTIONS

B.B.A., L.P.S., and W.P.M. conceived and designed research; B.B.A. performed experiments; B.B.A. analyzed data; B.B.A., L.P.S., W.I.V., R.J.P., and W.P.M. interpreted results of experiments; B.B.A., L.P.S., and W.P.M. prepared figures; B.B.A., L.P.S., and W.P.M. drafted manuscript; B.B.A., L.P.S., W.I.V., R.J.P., and W.P.M. edited and revised manuscript; B.B.A., L.P.S., W.I.V., R.J.P., and W.P.M. approved final version of manuscript.

REFERENCES

Alberts BB, de Brouwer AJ, Selen LP, Medendorp WP. A Bayesian account of visual-vestibular interactions in the rod-and-frame task. *eNeuro* 3: ENEURO.0093–16.2016, 2016. doi:10.1523/ENEURO.0093-16.2016.

Alberts BB, Selen LP, Verhagen WI, Medendorp WP. Sensory substitution in bilateral vestibular a-reflexic patients. *Physiol Rep* 3: e12385, 2015. doi:10.14814/phy2.12385.

Angelaki DE, Cullen KE. Vestibular system: the many facets of a multimodal sense. *Annu Rev Neurosci* 31: 125–150, 2008. doi:10.1146/annurev.neuro.31.060407.125555.

Angelaki DE, Yakusheva TA. How vestibular neurons solve the tilt/translation ambiguity. Comparison of brainstem, cerebellum, and thalamus. *Ann NY Acad Sci* 1164: 19–28, 2009. doi:10.1111/j.1749-6632.2009.03939.x.

Anson E, Jeka J. Perspectives on aging vestibular function. *Front Neurol* 6: 269, 2016. doi:10.3389/fneur.2015.00269.

Aubert H. Eine scheinbare bedeutende Drehung von Objecten bei Neigung des Kopfes nach rechts oder links. *Arch Pathol Anat Physiol Klin Med* 20: 381–393, 1861. doi:10.1007/BF02355256.

Bagust J. Assessment of verticality perception by a rod-and-frame test: preliminary observations on the use of a computer monitor and video eye glasses. *Arch Phys Med Rehabil* 86: 1062–1064, 2005. doi:10.1016/j.apmr.2004.05.022.

Beh H, Wenderoth P. The effect of variation of frame shape on the angular function of the rod-and-frame illusion. *Percept Psychophys* 11: 35–37, 1972. doi:10.3758/BF03212679.

Beh H, Wenderoth P, Purcell A. The angular function of a rod-and-frame illusion. *Percept Psychophys* 9: 353–355, 1971. doi:10.3758/BF03208694.

Bischoff AM, Huygen PL, Kemperman MH, Pennings RJ, Bom SJ, Verhagen WI, Admiraal RJ, Kremer H, Cremers CW. Vestibular deterioration precedes hearing deterioration in the P51S COCH mutation (DFNA9): an analysis in 74 mutation carriers. *Otol Neurotol* 26: 918–925, 2005. doi:10.1097/01.mao.0000185048.84641.e3.

Brandt T, Dieterich M. The vestibular cortex. Its locations, functions, and disorders. *Ann NY Acad Sci* 871: 293–312, 1999. doi:10.1111/j.1749-6632.1999.tb09193.x.

Bronstein AM. The interaction of otolith and proprioceptive information in the perception of verticality. The effects of labyrinthine and CNS disease. *Ann NY Acad Sci* 871: 324–333, 1999. doi:10.1111/j.1749-6632.1999.tb09195.x.

Bronstein AM, Hood JD. The cervico-ocular reflex in normal subjects and patients with absent vestibular function. *Brain Res* 373: 399–408, 1986. doi:10.1016/0006-8993(86)90355-0.

Bronstein AM, Yardley L, Moore AP, Cleeves L. Visually and posturally mediated tilt illusion in Parkinson's disease and in labyrinthine defective subjects. *Neurology* 47: 651–656, 1996. doi:10.1212/WNL.47.3.651.

Carriot J, Cian C, Paillard A, Denise P, Lackner JR. Influence of multisensory graviceptive information on the apparent zenith. *Exp Brain Res* 208: 569–579, 2011. doi:10.1007/s00221-010-2505-y.

Clark TK, Newman MC, Oman CM, Merfeld DM, Young LR. Human perceptual overestimation of whole body roll tilt in hypergravity. *J Neurophysiol* 113: 2062–2077, 2015. doi:10.1152/jn.00095.2014.

Clemens IA, De Vrijer M, Selen LP, Van Gisbergen JA, Medendorp WP. Multisensory processing in spatial orientation: an inverse probabilistic approach. *J Neurosci* 31: 5365–5377, 2011. doi:10.1523/JNEUROSCI.6472-10.2011.

Coppola DM, Purves HR, McCoy AN, Purves D. The distribution of oriented contours in the real world. *Proc Natl Acad Sci USA* 95: 4002–4006, 1998. doi:10.1073/pnas.95.7.4002.

Cremers CW, Kemperman MH, Bom SJ, Huygen PL, Verhagen WI, Kremer JM. [From gene to disease; a progressive cochlear-vestibular dysfunction with onset in middle-age (DFNA9)]. *Ned Tijdschr Geneeskd* 149: 2619–2621, 2005.

Cullen KE. The neural encoding of self-generated and externally applied movement: implications for the perception of self-motion and spatial memory. *Front Integr Neurosci* 7: 108, 2014. doi:10.3389/fnint.2013.00108.

Cullen KE, Minor LB, Beraneck M, Sadeghi SG. Neural substrates underlying vestibular compensation: contribution of peripheral versus central processing. *J Vestib Res* 19: 171–182, 2009. doi:10.3233/VES-2009-0357.

Curthoys IS. Vestibular compensation and substitution. *Curr Opin Neurol* 13: 27–30, 2000. doi:10.1097/00019052-200002000-00006.

Cutfield NJ, Scott G, Waldman AD, Sharp DJ, Bronstein AM. Visual and proprioceptive interaction in patients with bilateral vestibular loss. *Neuroimage Clin* 4: 274–282, 2014. doi:10.1016/j.nicl.2013.12.013.

De Vrijer M, Medendorp WP, Van Gisbergen JA. Shared computational mechanism for tilt compensation accounts for biased verticality percepts in motion and pattern vision. *J Neurophysiol* 99: 915–930, 2008. doi:10.1152/jn.00921.2007.

De Vrijer M, Medendorp WP, Van Gisbergen JA. Accuracy-precision trade-off in visual orientation constancy. *J Vis* 9: 1–15, 2009. doi:10.1167/9.2.9.

Deveze A, Bernard-Demanze L, Xavier F, Lavieille JP, Elziere M. Vestibular compensation and vestibular rehabilitation. Current concepts and new trends. *Neurophysiol Clin* 44: 49–57, 2014. doi:10.1016/j.neucli.2013.10.138.

Dieterich M, Bauermann T, Best C, Stoeter P, Schlindwein P. Evidence for cortical visual substitution of chronic bilateral vestibular failure (an fMRI study). *Brain* 130: 2108–2116, 2007. doi:10.1093/brain/awm130.

Eggert T. Segregation of visual features is not the basis of visual orientation relative to gravity. *Ann NY Acad Sci* 656: 836–837, 1992. doi:10.1111/j.1749-6632.1992.tb25268.x.

Eggert T. *Der Einfluss orientierter Texturen auf die subjektive visuelle Vertikale und seine systemtheoretische Analyse* (PhD thesis). Munich, Germany: Technische Univ. München, 1998.

Faisal AA, Selen LP, Wolpert DM. Noise in the nervous system. *Nat Rev Neurosci* 9: 292–303, 2008. doi:10.1038/nrn2258.

Fernández C, Goldberg JM. Physiology of peripheral neurons innervating otolith organs of the squirrel monkey. I. Response to static tilts and to long-duration centrifugal force. *J Neurophysiol* 39: 970–984, 1976. doi:10.1152/jn.1976.39.5.970.

Fiori F, Candidi M, Acciarino A, David N, Aglioti SM. The right temporo-parietal junction plays a causal role in maintaining the internal representation of verticality. *J Neurophysiol* 114: 2983–2990, 2015. doi:10.1152/jn.00289.2015.

Fransen E, Verstreken M, Bom SJ, Lemaire F, Kemperman MH, De Kok YJ, Wuyts FL, Verhagen WI, Huygen PL, McGuirt WT, Smith RJ, Van Maldergem LV, Declau F, Cremers CW, Van De Heyning PH, Cremers FP, Van Camp G. A common ancestor for COCH related cochleovestibular (DFNA9) patients in Belgium and The Netherlands bearing the P51S mutation. *J Med Genet* 38: 61–65, 2001. doi:10.1136/jmg.38.1.61.

Girshick AR, Landy MS, Simoncelli EP. Cardinal rules: visual orientation perception reflects knowledge of environmental statistics. *Nat Neurosci* 14: 926–932, 2011. doi:10.1038/nn.2831.

Grabherr L, Cuffel C, Guyot JP, Mast FW. Mental transformation abilities in patients with unilateral and bilateral vestibular loss. *Exp Brain Res* 209: 205–214, 2011. doi:10.1007/s00221-011-2535-0.

Gresty MA, Hess K, Leech J. Disorders of the vestibulo-ocular reflex producing oscillopsia and mechanisms compensating for loss of labyrinthine function. *Brain* 100: 693–716, 1977. doi:10.1093/brain/100.4.693.

Guerraz M, Poquin D, Luyat M, Ohlmann T. Head orientation involvement in assessment of the subjective vertical during whole body tilt. *Percept Mot Skills* 87: 643–648, 1998. doi:10.2466/pms.1998.87.2.643.

Guerraz M, Yardley L, Bertholon P, Pollak L, Rudge P, Gresty MA, Bronstein AM. Visual vertigo: symptom assessment, spatial orientation and postural control. *Brain* 124: 1646–1656, 2001. doi:10.1093/brain/124.8.1646.

Guinand N, Van de Berg R, Cavuscens S, Stokroos R, Ranieri M, Pelizzone M, Kingma H, Guyot JP, Pérez Fornos A. Restoring visual acuity in dynamic conditions with a vestibular implant. *Front Neurosci* 10: 577, 2016. doi:10.3389/fnins.2016.00577.

Herdman SJ. Vestibular rehabilitation. *Curr Opin Neurol* 26: 96–101, 2013. doi:10.1097/WCO.0b013e32835c5ec4.

Herdman SJ, Schubert MC, Das VE, Tusa RJ. Recovery of dynamic visual acuity in unilateral vestibular hypofunction. *Arch Otolaryngol Head Neck Surg* 129: 819–824, 2003. doi:10.1001/archotol.129.8.819.

Hillier SL, McDonnell M. Vestibular rehabilitation for unilateral peripheral vestibular dysfunction. *Cochrane Database Syst Rev* 2: CD005397, 2011. doi:10.1002/14651858.CD005397.pub3.

Huygen PL, Verhagen WI. Optokinetic response in patients with vestibular areflexia. *J Vestib Res* 21: 219–225, 2011.

Huygen PL, Verhagen WI, Nicolasen MG. Cervico-ocular reflex enhancement in labyrinthine-defective and normal subjects. *Exp Brain Res* 87: 457–464, 1991. doi:10.1007/BF00231863.

Huygen PL, Verhagen WI, Theunissen EJ, Nicolasen MG. Compensation of total loss of vestibulo-ocular reflex by enhanced optokinetic response. *Acta Otolaryngol Suppl* 468: 359–364, 1989. doi:10.3109/00016488909139077.

Jamali M, Mitchell DE, Dale A, Carriot J, Sadeghi SG, Cullen KE. Neuronal detection thresholds during vestibular compensation: contributions of response variability and sensory substitution. *J Physiol* 592: 1565–1580, 2014. doi:10.1113/jphysiol.2013.267534.

Kasai T, Zee DS. Eye-head coordination in labyrinthine-defective human beings. *Brain Res* 144: 123–141, 1978. doi:10.1016/0006-8993(78)90439-0.

Kitahara T, Takeda N, Kiyama H, Kubo T. Molecular mechanisms of vestibular compensation in the central vestibular system—review. *Acta Otolaryngol Suppl* 539: 19–27, 1998. doi:10.1080/00016489850182071.

Lackner JR, DiZio P. Vestibular, proprioceptive, and haptic contributions to spatial orientation. *Annu Rev Psychol* 56: 115–147, 2005. doi:10.1146/annurev.psych.55.090902.142023.

Laurens J, Kim B, Dickman JD, Angelaki DE. Gravity orientation tuning in macaque anterior thalamus. *Nat Neurosci* 19: 1566–1568, 2016. doi:10.1038/nn.4423.

Lester BD, Dassonville P. The role of the right superior parietal lobule in processing visual context for the establishment of the egocentric reference frame. *J Cogn Neurosci* 26: 2201–2209, 2014. doi:10.1162/jocn_a_00636.

Lewis RF. Advances in the diagnosis and treatment of vestibular disorders: psychophysics and prosthetics. *J Neurosci* 35: 5089–5096, 2015. doi:10.1523/JNEUROSCI.3922-14.2015.

Li W, Matin L. The rod-and-frame effect: the whole is less than the sum of its parts. *Perception* 34: 699–716, 2005a. doi:10.1068/p5411.

Li W, Matin L. Visually perceived vertical (VPV): induced changes in orientation by 1-line and 2-line roll-tilted and pitched visual fields. *Vision Res* 45: 2037–2057, 2005b. doi:10.1016/j.visres.2005.01.014.

Lopez C, Lacour M, Ahmadi AE, Magnan J, Borel L. Changes of visual vertical perception: a long-term sign of unilateral and bilateral vestibular loss. *Neuropsychologia* 45: 2025–2037, 2007. doi:10.1016/j.neuropsychologia.2007.02.004.

MacNeilage PR, Banks MS, Berger DR, Bülthoff HH. A Bayesian model of the disambiguation of gravitoinertial force by visual cues. *Exp Brain Res* 179: 263–290, 2007. doi:10.1007/s00221-006-0792-0.

Mars F, Popov K, Vercher JL. Supramodal effects of galvanic vestibular stimulation on the subjective vertical. *Neuroreport* 12: 2991–2994, 2001. doi:10.1097/00001756-200109170-00047.

Mars F, Vercher JL, Blouin J. Perception of the vertical with a head-mounted visual frame during head tilt. *Ergonomics* 47: 1116–1130, 2004. doi:10.1080/00140130410001695933.

Matin L, Li W. Multimodal basis for egocentric spatial localization and orientation. *J Vestib Res* 5: 499–518, 1995. doi:10.1016/0957-4271(95)02003-B.

McCall AA, Yates BJ. Compensation following bilateral vestibular damage. *Front Neurol* 2: 88, 2011. doi:10.3389/fneur.2011.00088.

McDonnell MN, Hillier SL. Vestibular rehabilitation for unilateral peripheral vestibular dysfunction. *Cochrane Database Syst Rev* 1: CD005397, 2015. doi:10.1002/14651858.CD005397.pub4.

Merfeld DM. Signal detection theory and vestibular thresholds: I. Basic theory and practical considerations. *Exp Brain Res* 210: 389–405, 2011. doi:10.1007/s00221-011-2557-7.

Mittelstaedt H. A new solution to the problem of the subjective vertical. *Naturwissenschaften* 70: 272–281, 1983. doi:10.1007/BF00404833.

Mittelstaedt H. Somatic versus vestibular gravity reception in man. *Ann NY Acad Sci* 656: 124–139, 1992. doi:10.1111/j.1749-6632.1992.tb25204.x.

Mittelstaedt H. Evidence of somatic graviception from new and classical investigations. *Acta Otolaryngol Suppl* 520: 186–187, 1995. doi:10.3109/00016489509125224.

Mittelstaedt H. Somatic graviception. *Biol Psychol* 42: 53–74, 1996. doi:10.1016/0301-0511(95)05146-5.

Popov K, Lekhel H, Bronstein A, Gresty M. Postural responses to vibration of neck muscles in patients with unilateral vestibular lesions. *Neurosci Lett* 214: 202–204, 1996. doi:10.1016/0304-3940(96)12909-8.

Robertson NG, Cremers CW, Huygen PL, Ikezono T, Krastins B, Kremer H, Kuo SF, Liberman MC, Merchant SN, Miller CE, Nadol JB Jr, Sarracino DA, Verhagen WI, Morton CC. Cochlin immunostaining of inner ear pathologic deposits and proteomic analysis in DFNA9 deafness and vestibular dysfunction. *Hum Mol Genet* 15: 1071–1085, 2006. doi:10.1093/hmg/ddl022.

Sadeghi SG, Minor LB, Cullen KE. Neural correlates of sensory substitution in vestibular pathways following complete vestibular loss. *J Neurosci* 32: 14685–14695, 2012. doi:10.1523/JNEUROSCI.2493-12.2012.

Santos-Pontelli TE, Rimoli BP, Favoretto DB, Mazin SC, Truong DQ, Leite JP, Pontes-Neto OM, Babyar SR, Reding M, Bikson M, Edwards DJ. Polarity-dependent misperception of subjective visual vertical during and after transcranial direct current stimulation (tDCS). *PLoS One* 11: e0152331, 2016. doi:10.1371/journal.pone.0152331.

Sober SJ, Körding KP. What silly postures tell us about the brain. *Front Neurosci* 6: 154, 2012. doi:10.3389/fnins.2012.00154.

Tarnutzer AA, Bockisch CJ, Straumann D. Roll-dependent modulation of the subjective visual vertical: contributions of head- and trunk-based signals. *J Neurophysiol* 103: 934–941, 2010. doi:10.1152/jn.00407.2009.

Tjernström F, Zur O, Jahn K. Current concepts and future approaches to vestibular rehabilitation. *J Neurol* 263, *Suppl* 1: S65–S70, 2016. doi:10.1007/s00415-015-7914-1.

Van Barneveld DC, Van Grootel TJ, Alberts B, Van Opstal AJ. The effect of head roll on perceived auditory zenith. *Exp Brain Res* 213: 235–243, 2011. doi:10.1007/s00221-011-2741-9.

van der Schaaf A, van Hateren JH. Modelling the power spectra of natural images: statistics and information. *Vision Res* 36: 2759–2770, 1996. doi:10.1016/0042-6989(96)00002-8.

Verhagen WI, Bom SJ, Huygen PL, Fransen E, Van Camp G, Cremers CW. Familial progressive vestibulocochlear dysfunction caused by a COCH mutation (DFNA9). *Arch Neurol* 57: 1045–1047, 2000. doi:10.1001/archneur.57.7.1045.

Vingerhoets RA, De Vrijer M, Van Gisbergen JA, Medendorp WP. Fusion of visual and vestibular tilt cues in the perception of visual vertical. *J Neurophysiol* 101: 1321–1333, 2009. doi:10.1152/jn.90725.2008.

Volkening K, Bergmann J, Keller I, Wuehr M, Müller F, Jahn K. Verticality perception during and after galvanic vestibular stimulation. *Neurosci Lett* 581: 75–79, 2014. doi:10.1016/j.neulet.2014.08.028.

Walter E, Dassonville P. Visuospatial contextual processing in the parietal cortex: an fMRI investigation of the induced Roelofs effect. *Neuroimage* 42: 1686–1697, 2008. doi:10.1016/j.neuroimage.2008.06.016.

Weber KP, Aw ST, Todd MJ, McGarvie LA, Curthoys IS, Halmagyi GM. Head impulse test in unilateral vestibular loss: vestibulo-ocular reflex and catch-up saccades. *Neurology* 70: 454–463, 2008. doi:10.1212/01.wnl.0000299117.48935.2e.

Wei XX, Stocker AA. A Bayesian observer model constrained by efficient coding can explain "anti-Bayesian" percepts. *Nat Neurosci* 18: 1509–1517, 2015. doi:10.1038/nn.4105.

Wichmann FA, Hill NJ. The psychometric function: I. Fitting, sampling, and goodness of fit. *Percept Psychophys* 63: 1293–1313, 2001. doi:10.3758/BF03194544.

Witkin HA, Asch SE. Studies in space orientation. IV. Further experiments on perception of the upright with displaced visual fields. *J Exp Psychol* 38: 762–782, 1948. doi:10.1037/h0053671.